DEFORMATION BEHAVIOR ANALYSES OF BRACED EXCAVATION CONSIDERING ADJACENT STRUCTURE BY USER-DEFINED SOIL MODELS

Huu-Phuoc Dang [1], Horn-Da Lin [2], Johnson H. S. Kung [3], and Chien-Chih Wang [4]

ABSTRACT

This paper documents a study on deformation characteristics of a braced excavation, in which the excavation process was performed by zoned approach, with consideration of neighboring structure through the in-situ measurement and numerical analysis. The field observations indicate that the wall and ground displacement behavior induced by the zoned excavation approach is similar to those resulted from conventional excavation method as the measured values can be predicted properly by empirical methods based on the traditional excavation. In addition, the deviation between the building deformation and the greenfield ground settlement is examined by means of the settlement ratio between those two quantities. This ratio is found to vary within a small range. Furthermore, the excavation-induced building settlement is studied to examine the properness of a proposed building simulation method in the literature. Then, the effects of building properties including weight and rigidity on the building deformations are evaluated. Study on the obtained results provides a valuable insight regarding how to enhance the accuracy of building simulation in numerical analysis and what the excavation-induced building responses can be expected.

Key words: Numerical analysis, braced excavation, adjacent structure, user-defined soil model, excavation response.

1. INTRODUCTION

Conventional braced excavation responses have been investigated by a number of studies (Wong and Brom 1989; Ou *et al*. 1998; Ou *et al*. 2000; Finno *et al*. 2002; Kung *et al*. 2007). On the other hand, study on the performance of the braced construction with the zoned excavation method is still limited. The zoned excavation method is often applied in relatively large construction site where the execution area is separated into smaller zones and the excavation process is then performed zone by zone. The excavation procedure in each zone is similar to conventional approach. Therefore, the performances of the zoned and traditional braced excavations, including wall and ground displacements, are supposed to be closely related and worthwhile for further investigation.

In addition, the excavation-induced damage of adjacent structures is an important issue in the analysis and design of an excavation project. There are numerous studies in this regard (Boscardin and Cording 1989; Boone 1996; Son and Cording 2005; Schuster *et al*. 2009). The fundamental requirement of these studies is the deformation of the structure. On this subject, the excavation-induced or tunneling-induced structure deformation has been examined by means of numerical analysis (Potts and Addenbrooke 1997; Burd *et al*. 2000) and physical test (Son and Cording 2005; Laefer *et al*. 2009). Although significant progress has been made; much more effort is still needed for better simulation of the excavation-induced building response. In this study the method proposed by Potts and Addenbrooke (1997) is evaluated using a field case in Taiwan.

Numerical analysis of excavation cases by means of finite element method (FEM) has been reported in the literature (Hsieh *et al*. 2003; Hsieh and Ou 1997; Finno *et al*. 2002; Kung *et al*. 2007). Most cases have been analyzed in two-dimensional condition. This study also adopts a two-dimensional-based FEM solution in the analysis. However, the construction procedure and field measurement of a zoned excavation cannot be readily employed for the analysis due to the spatial characteristic of excavation procedure. Therefore, the present paper utilizes the method reported by Lin *et al*. (2011) to simplify the excavation sequence and measurement into plane strain-based data. In addition, Kung *et al*. (2007) pointed out the necessity of using advanced or small strain soil model to enhance the accuracy of the analytical result. As a result, this study also adopts these advanced soil models in the analysis.

2. EXCAVATION CASE HISTORY

2.1 Case Overview

This study adopts the zoned excavation case reported by Lin *et al*. (2011). Figure 1 illustrates the excavation plan of three excavation zones including *A*, *B*, and *C* and a simplified excavation section. The excavation responses as well as existing structure deformation behavior were monitored by a series of measured instruments equipped at interested sections and buildings.

Manuscript received June 3, 2011; revised October 22, 2011; accepted February 13, 2012.

[1] Ph.D. Candidate, Department of Construction Engineering, National Taiwan University of Science and Technology, Taipei, Taiwan.

[2] Professor (corresponding author), Department of Construction Engineering, National Taiwan University of Science and Technology, Taipei, Taiwan (e-mail: hdlin@mail.ntust.edu.tw).

[3] Former Ph.D. Candidate, Department of Construction Engineering, National Taiwan University of Science and Technology, Taipei, Taiwan.

[4] Associate Professor, Department of Civil Engineering and Engineering Informatics, Cheng Shiu University, Kaohsiung, Taiwan.

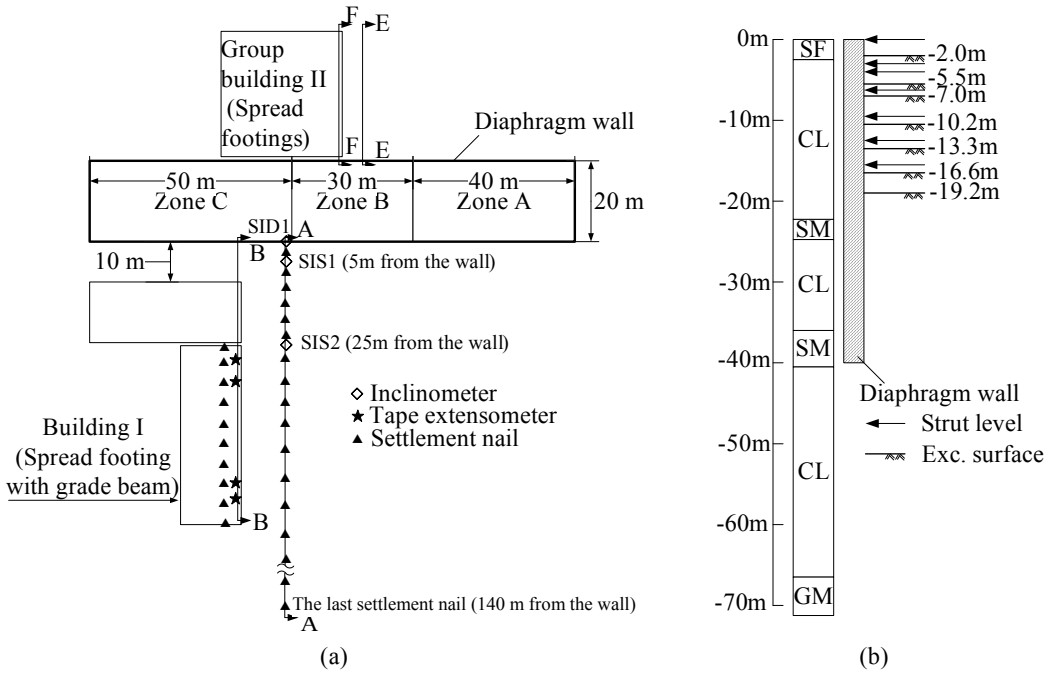

Fig. 1 Excavation profile: (a) Instrumentation plan; (b) Simplified excavation section

To increase the accuracy and reliability of onsite readings the inclinometer embedded in the diaphragm wall was elongated about 20 m below the bottom of the wall and embedded in the stiff soil layer. It should be noted that two building groups next to the excavation zone (building I and group building II) are low rise framed structures. In which, the building I is 4-story building and group building II are 1-to-3-story buildings. All the structures are supported by spread footings.

The 6-layer soil profile and the property of each layer are illustrated in Table 1. The top layer with thickness of 1 m was sand fill. The hard rock positioned at the depth of 67.5 m. In between, the soil was composed of alternating clay and sand layers. The N-value and friction angle (ϕ') increased constantly with depth, in which ϕ' ranged from 30 to 35 degrees. It should be noted that all the excavation activities were conducted in the soft clay layer right beneath the sand fill layer with relatively small values of SPT-N and shear strength. Thus, this layer is expected to have predominant influence on wall, ground, and structure responses.

The excavation was supported by a 1-m-thick and 40-m-deep diaphragm wall as shown in Fig. 1(b). The H steel strut with prestressed loading and horizontal spacing of about 5 m was utilized. Moreover, the soil at the depth of 19 m to 22 m was strengthened by using jumbo special grouting (JSG) technique to form a wall-type soil improvement. Table 2 summarizes the excavation depths of zones A, B, and C sequentially. Generally, all zones were excavated simultaneously to the depth of 2 m for the installation of the decking beam used to support the deck for maintaining traffic. Then, the zones were excavated respectively until the final depth of 19.2 m. It should be emphasized that the excavation depths in each zone were nearly similar although the cutting was conducted at different time. It is the key finding for the simplification approach that will be mentioned in the later section.

Table 1 Soil properties at the excavation site (after Lin *et al.* 2011)

Depth (m)	Classification	SPT	γ (kN/m^3)	ϕ' (degree)
0 ~ 1.0	SF*	5	19.5	30
1.0 ~ 22.2	CL	3 ~ 6	18.6	30
22.2 ~ 24.6	SM	13	19.0	31
24.6 ~ 35.6	CL	10 ~ 15	19.1	33
35.6 ~ 40.2	SM	17	19.2	35
40.2 ~ 67.5	CL	25	18.9	33

* SF: Surface fill

2.2 Field Observations and Discussions

Lin *et al*. (2011) reported a general account of field measurements of excavation responses at all instrumented sections. More in-depth discussions will be made in this paper. Within the scope of the present study only the results of deformations along section A and building I are adopted as they will be analyzed elaborately in later analysis.

Figure 2 illustrates the lateral displacements of diaphragm wall (SID1) and soil (SIS1 at 5 m from the wall and SIS 2 at 25 m from the wall). It is observed that the movement trends of this zoned excavation case at three locations are similar to those of conventional excavation. At the locations of SID1 and SIS1 the lateral movements behaved in a cantilever mode in the early

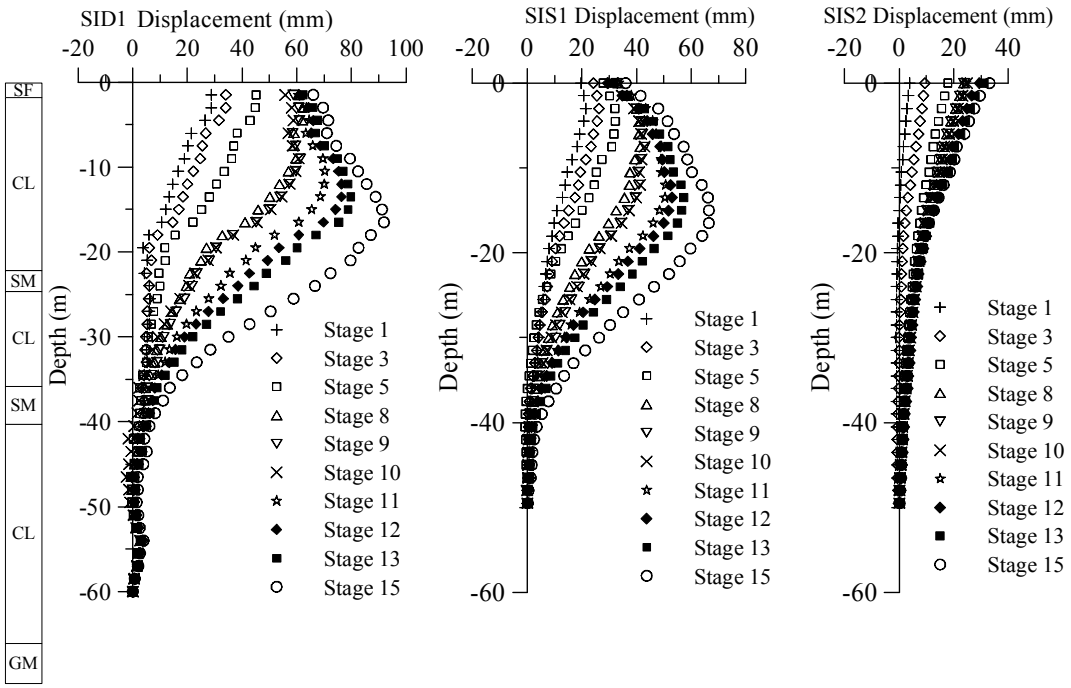

Fig. 2 Lateral displacement at SID1, SIS1, and SIS2

Table 2 Zoned excavation sequence (Lin *et al.* 2011)

Stage	Excavation depth (m)		
	Zone C	Zone B	Zone A
1	**2**	**2**	**2**
2	2	2	***4.6***
3	2	***5.5***	***5.5***
4	2	***7.0***	***7.0***
5	2	***10.2***	***10.2***
6	***5***	10.2	10.2
7	***6***	10.2	10.2
8	***7.6***	10.2	10.2
9	7.6	***13.3***	***13.3***
10	***10.5***	13.3	13.3
11	10.5	***16.6***	***16.6***
12	***13.6***	16.6	16.6
13	13.6	***19.2***	***19.2***
14	***16.6***	19.2	19.2
15	***19.2***	19.2	19.2

Note: The italic and bold numbers indicate the excavation was processed in that zone

stages. As the excavation proceeded and the top of the wall was propped, larger inward movement occurred near the excavation surface. Therefore, at later stages the maximum displacements took place slightly above the excavation depths. Therefore, as shown in Fig. 3 the spandrel and concave types of ground settlement were observed at the early and the later stages, respectively.

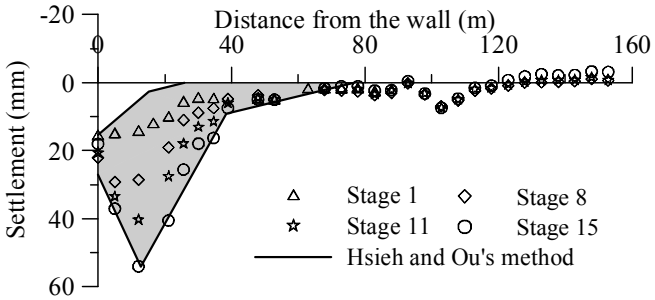

Fig. 3 Ground settlement and empirical prediction at section *A*

On the other hand, the soil at SIS2 displaced as a cantilever for all stages as SIS2 positioned far from the wall.

Moreover, based on Fig. 2 it is fair to say that the measurements at SID1, SIS1, and SIS2 are consistent with each other. The reading of inclinometers was the largest at the diaphragm wall and the smallest at SIS2 as the influence of the excavation process was reduced with increase of distance. Moreover, SIS1 was positioned quite close to the wall; therefore, the overall trend of obtained movements at SIS1 was similar to that of SID1; for example, the maximum deflections of SID1 and SIS1 occurred at the same depth at various excavation stages and movement sequence at the ground surface level was coincident as the displacements all kept increasing until stage 8 and became steady afterward.

Together with the overall deformation trends, the amplitudes of wall and ground displacements of the zoned excavation can also be predicted by empirical measure derived from conventional excavation procedure. For instance, the maximum wall deflection (δ_{hm}) at final stage was 92 mm; it was about 0.48% of corresponding excavation depth (H_e = 19.2 m). This value is in the range of 0.2% to 0.5% H_e proposed by Ou (2006). Further, the maximum ground settlement (δ_{vm}) was 54 mm; therefore, the

ratio of δ_{vm} and δ_{hm} was 59% and stayed in the range of 50% to 75% suggested by Ou (2006). As shown in Fig. 3 the ground settlement trough can be predicted properly by an empirical method of Hsieh and Ou (1998).

Nevertheless, it can be seen that relatively large wall movement obtained near the ground surface as shown in Fig. 2 seemed to be beyond that would be expected. This phenomenon would be attributed to some unexpected causes such as inappropriate workmanship or non-proper function of the bracing system in the early excavation stages. Moreover, as there was a relatively long waiting period right after some early excavation stages, the creep effect might also contribute to the additional movement at the top of the wall according to a study by Lin *et al*. (2002).

As far as the adjacent building is concerned, the settlement variation of building I, a spread footing with grade beam structure, is shown in Fig. 4. The differential settlement became more profound at later stages as the corner of the building near the wall settled more significantly than the far end. Moreover, it can be seen that building movements were much larger than ground settlements in greenfield condition at the same location. To quantify that deviation, the amplification factor defined as the ratio of building settlement and ground settlement is adopted. Figure 5(a) demonstrates an obvious example of settlement difference between ground and building at final stage. At various excavation stages, the amplification factor varies in the range of 2 to 4 as shown in Fig. 5(b). It should be noted that the range of 2 to 4 in this study is only valid for the low rise concrete framed building supported on spread footings with grade beam. More studies are needed to examine this range. However, this value offers an idea about how much the ground settlement can be modified if there is an existing structure. Moreover, it also implies that if the greenfield ground settlement, not the building settlement, is used to evaluate the building condition, this computation practice may mislead the building damage potential.

The deviation of ground and building settlements can also be found in the works of Potts and Addenbrooke (1997) and Son and Cording (2005). However, the quantification of that deviation was not clearly indicated therein. Intuitively, this difference may depend upon the foundation type, building rigidity, and building weight. For example, the spread footing may settle independently while the mat foundation functions in an interconnected manner. The rigidity variation may affect the shape of settlement trough meanwhile the building weight may cause variation in settlement amplitude.

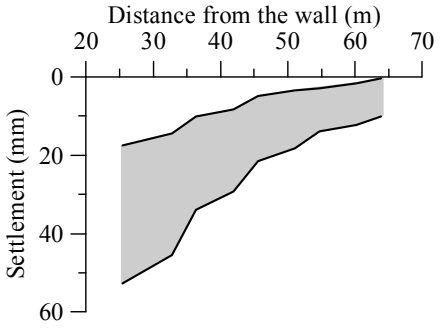

Fig. 4 Building I settlement envelope

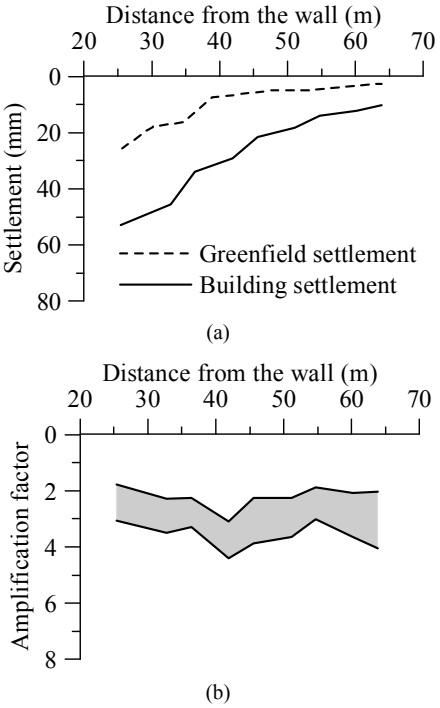

Fig. 5 (a) Deviation of greenfield and building settlements at final stage; (b) Variation of amplification factor

3. NUMERICAL PROCEDURE FOR 2D ANALYSIS

As shown in Table 2, the zoned excavation procedure is basically a three-dimensional scheme. In other words, at a certain stage, the excavation depths in zones A, B, and C were different. However, in a plane strain analysis, the soil is assumed to be excavated simultaneously. Therefore, to analyze this case history by a plane-strain-based FEM solution it is necessary to simplify the zoned excavation sequence and associated field measurements into two-dimensional sequence and measurements. Based on a general concept proposed by Lin *et al*. (2001), the simplified scheme is summarized as follows:

1. Determine the primary zones according to the excavation property. The primary zone is defined as the zone that has predominant effect on wall and ground movements
2. Select typical excavation depth of each simplified stage; for simplicity, it should be the depth of primary zones
3. Identify the actual field measurement when the excavation is conducted to the typical depth in the primary zones
4. Evaluate the effect of secondary zones on the field measurement once the excavation in secondary zones approaches the typical depth
5. Combine the measurement and additional effect as it will represent simplified measurement for all zones at the typical excavation depth

The simplified construction procedure of this case history is described in Table 3. Hereafter, the excavation stage is referred as the simplified excavation stage.

Table 3 Simplified excavation procedure

Order	Task	Ground level (m)
1	Shallow excavation (Simplified excavation stage 1)	–2
2	Install decking beam	0
3	Excavation (Simplified excavation stage 2)	–5.5
4	Install strut H350 × 350 × 12 × 19 with preload 60 t/strut, space = 5 m	–2.4
5	Install strut 2-H350 × 350 × 12 × 19 with preload 50 t/strut, space = 5 m	–4.0
6	Excavation (Simplified excavation stage 3)	–7.0
7	Install strut 2-H400 × 400 × 13 × 21 with preload 80 t/strut, space = 5 m	–6.1
8	Excavation (Simplified excavation stage 4)	–10.2
9	Install strut 2-H428 × 407 × 20 × 35 with preload 125 t/strut, space = 5 m	–9.1
10	Excavation (Simplified excavation stage 5)	–13.3
11	Install strut 2-H428 × 407 × 20 × 35 with preload 140 t/strut, space = 5 m	–12.3
12	Excavation (Simplified excavation stage 6)	–16.6
13	Install strut 2-H428 × 407 × 20 × 35 with preload 150 t/strut, space = 5 m	–15.5
14	Excavation (Simplified excavation stage 7)	–19.2

As far as the numerical tool is concerned, this study adopts PLAXIS, a FEM solution, in analysis. Although PLAXIS is not an open-source tool, it enables the user to embed the constitutive soil model. The user-defined soil model needs to be programmed in a programming language then added into the PLAXIS' directory. The details of programming procedure can be referred to Dang *et al*. (2010); herein only the numerical outcome is introduced. In the work of Dang *et al*. (2010), the modified pseudo plasticity (MPP) small strain model developed by Hsieh *et al*. (2003) and later modified by Hsieh and Ou (2011) and hyperbolic model proposed by Duncan and Chang (1970) were implemented successfully in PLAXIS.

In general, MPP model was developed for clayey soil based on the concept of hyperbolic model. It can capture the behavior of nonlinearity, anisotropy, small strain, and degradation of soil stiffness. Parameters of MPP model consist of E_i / s_{uc} and s_{uc} / σ'_v, a, b, ν_u, R_f, and K_s. The ratios of E_i / s_{uc} and s_{uc} / σ'_v are adopted to determine the initial stiffness at small strain of the soil and undrained shear strength based on the effective vertical stress; the values of a and b control the stiffness degradation characteristic; undrained Poisson's ratio ν_u is equal to 0.495; R_f is the failure ratio; and K_s is the ratio of extension and compression undrained shear strengths. Meanwhile, the input parameters of hyperbolic model mainly include K, K_{ur}, n, ν', R_f, c', and ϕ' (degree). In which, K, K_{ur}, n are used to calculate the initial tangent modulus of the soil according to the theory of hyperbolic model; ν' is effective stress Poisson's ratio; R_f is failure ratio; c' and ϕ' are cohesion and friction angle, respectively.

The reasonable application of these user-defined soil models has been validated by laboratory results and excavation simulations. Dang *et al*. (2010) demonstrated the excellent agreement between analytical and tested stress-strain curves for both sand (hyperbolic model) and clay soils (MPP model) under loading and unloading-reloading conditions. As an extra work, these models were further adopted in a well-documented case history *i.e.*, Taipei National Enterprise Center (TNEC). The analytical wall and ground deformations fitted field measurements well.

4. ANALYSES AND DISCUSSIONS

4.1 Greenfield Condition

Due to the symmetrical excavation geometry along its width, only a half width is modeled by means of PLAXIS with user-defined soil models. The numerical mesh with detailed dimension is shown in Fig. 6. The dimension in the vertical direction is equal to the thickness of soil layers meanwhile the length of the model is selected according to the suggestion of Ou (2006). The soil elements are 15-node elements. The two side boundaries are constrained laterally or the roller fixity is applied. The bottom boundary displacement is restrained in both vertical and horizontal directions. Moreover, to increase the effectiveness of computational process the region close to the excavation zone is meshed finer than others. It should be noted that the beam which simulates adjacent building is not activated in the greenfield analysis.

In this study, the logic to determine the input parameters is to select the value within reasonable range that can best approximate the field measurements such that the subsequent analyses of adjacent building's response can be proceeded on a reasonable basis. Therefore, the input parameters of sandy and clayey soils are determined by calibrating from soil properties as shown in Table 1 and laboratory tests and by referring to former studies. The detailed values are illustrated in Tables 4 and 5. In which, the K and K_{ur} for sandy soil were derived from SPT-N values. The ratio of undrained shear strength and effective vertical stress (s_{uc} / σ'_v) was determined from the experiments. The s_{uc} / σ'_v value of 0.26, which is close to the lower bound of the testing results, is used for the top clayey layer meanwhile 0.28 is adopted for lower clayey layers as higher SPT-N value and friction angle were obtained in lower stratums. In addition, the small strain parameters for clay and hyperbolic parameters for both sand and clay were determined based on the results reported by Kung *et al*. (2007) and Hsieh *et al*. (2003).

Moreover, it should be noted that the soil improvement by JSG technique as described previously is excluded in the numerical analysis. It was found that there were many uncertainties during the soil improvement process. Further, the field measurements indicated that the soil improvement did not help to significantly reduce the wall and ground deformations. Therefore, by engineering judgment and for simplicity the numerical analysis did not take into account the soil improvement effect.

Figure 7 compares the predicted wall and ground displacements by PLAXIS with field measurements at various simplified excavation stages. In terms of wall deflection, the overall deformation trends between analytical results and onsite observations agree with each other. Moreover, the maximum wall displacement is approximated relatively well as summarized in Fig. 8. However, Fig. 7 does show some variations in deformation pattern near the ground surface. Several possible in-situ conditions that may cause the deviations have been described in section 2.2.

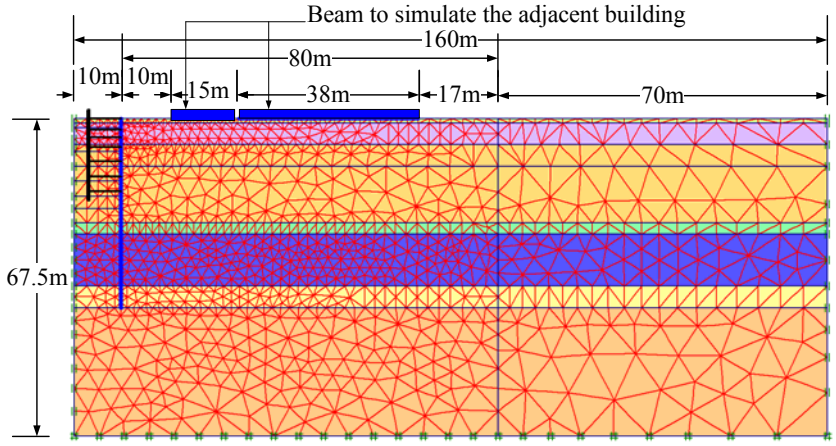

Fig. 6 Numerical mesh of the excavation study

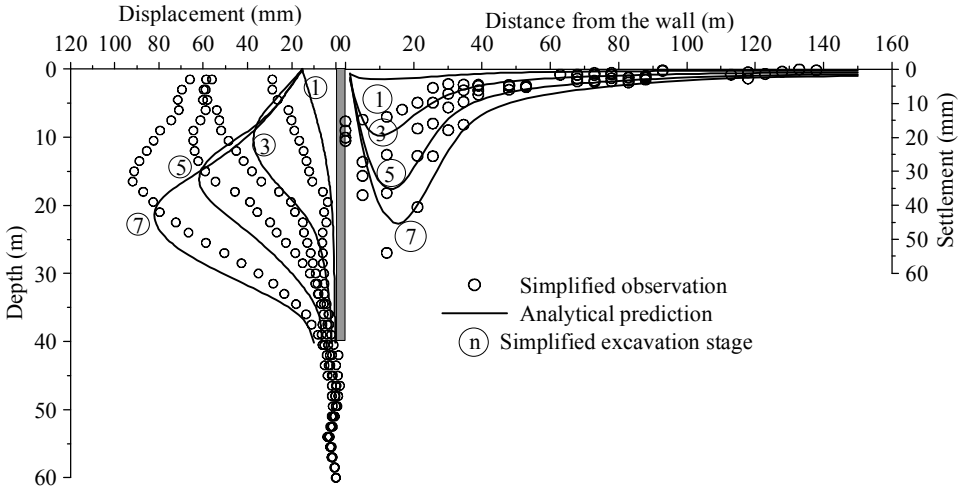

Fig. 7 Comparison of numerical and simplified measured wall and ground deformations

Table 4 Input parameters for sandy soils in analysis

Depth (m)	K	K_{ur}	n	ν′	R_f	c (kPa)	ϕ (degrees)
0 ~ 1	550	550	0.5	0.3	0.9	0	30
22.2 ~ 24.6	1350	1350	0.5	0.3	0.9	0	31
35.6 ~ 40.2	1800	1800	0.5	0.3	0.9	0	35

Table 5 Input parameters for clayey soils in analysis

Depth (m)	E_i / S_{uc}	S_{uc}	a	b	ν	R_f	K_s
1 ~ 5.5	2100	17 (kPa)	1×10^{-4}	1.4	0.495	0.9	0.8
5.5 ~ 22.2	2100	0.26 σ′$_v$	1×10^{-4}	1.4	0.495	0.9	0.8
24.6 ~ 35.6	2100	0.28 σ′$_v$	1×10^{-4}	1.4	0.495	0.9	0.8
40.2 ~ 67.5	2100	0.28 σ′$_v$	1×10^{-4}	1.4	0.495	0.9	0.8

In contrast to wall deflection, Figs. 7 and 8 express better agreements of predicted and observed ground settlement in terms of both deformation pattern as well as maximum value. Nevertheless, there is a little difference in the location of the largest settlement; it may be resulted from the deviation in wall movement.

4.2 Investigation of the Adjacent Building

Once the feasibility of greenfield analysis is demonstrated, the effect of the existing structure can be evaluated. Potts and Addenbrooke (1997) proposed a modeling approach that considered the building as a weightless beam on the ground surface. The beam stiffness included equivalent axial stiffness ($E_{eq}A_{eq}$) and bending stiffness ($E_{eq}I_{eq}$) that can be represented as $E_{eq}A_{eq} = (E_cA)_{struct}$ and $E_{eq}I_{eq} = (E_cI)_{struct}$; in which, $(E_cA)_{struct}$ and $(E_cI)_{struct}$ represented the structure stiffness and were derived from all building slabs. This method has been satisfactorily adopted by Burland *et al*. (2001) to evaluate the building settlement induced by underground tunneling during the construction of the Jubilee Line subway extension project in London. Although this method is a simplified approach and should be used with caution, it indeed provides a convenient tool for preliminary assessment of the excavation-induced building settlement. Therefore, the present paper adopts this method in the building simulation; nevertheless, the effect of building's rigidity and weight will be further examined.

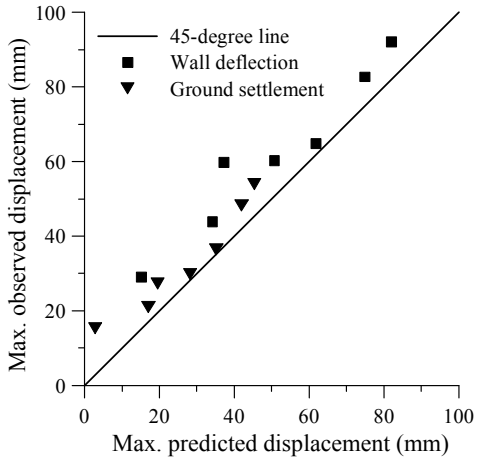

Fig. 8 Comparison of maximum wall and ground deformations at various excavation depths

According to Potts and Addenbrooke (1997), the equivalent axial stiffness ($E_{eq}A_{eq}$) and bending stiffness ($E_{eq}I_{eq}$) of the beam can be computed as follows:

1. Axial stiffness $E_{eq}A_{eq} = (E_cA)_{struct} = E_c\sum A_{slab}$ where E_c is concrete modulus and A_{slab} is the cross-sectional area of the individual slab
2. Bending stiffness $E_{eq}I_{eq} = (E_cI)_{struct} = E_c\sum(I_{slab} + A_{slab}H^2)$ where I_{slab} is the second moment of each slab and H is the vertical distance from the individual slab to the neutral axis

However, intuitively the equivalent stiffness calculated by summing stiffness from all slabs is somewhat overestimated because the deformability of each floor is different. Lower slabs are expected to deform more than upper slabs. Therefore, the present study examines the effect of the building stiffness by varying the bending stiffness with 10%, 1%, and 0.1% of the full stiffness computed by the above approach. Moreover, the self weight of the building always exists on the structure during its functioning period. Nevertheless, it was ignored in Potts and Addenbrooke's method. Thus, it is also of interest to investigate the effect of the self weight on the building settlement.

As mentioned previously, building I, a 4-story building supported by spread footings with grade beam, is investigated. The thicknesses of every floor slabs are assumed to be 0.15 m. The story height is 3.6 m. According to the above calculation procedure, the computed values of axial stiffness ($E_{eq}A_{eq}$) and bending stiffness ($E_{eq}I_{eq}$) are equal to 1.14×10^7 m^2/m and 2.96×10^8 m^4/m, respectively. In addition, the weight of the building is derived from its self weight such as wall, slab, column, and beam and 50% of the live load. Herein, the live load is reduced as the live load did not exist fully all the time. The total weight including dead load and live load of each floor is calculated to be equal to 11 kN/m^2. The roof slab is supposed to sustain a smaller live load; thus, total weight of the roof would be 10 kN/m^2. Therefore, the weight of the representing beam, including 4 floor slabs and one roof, is 54 kN/m/m.

The numerical mesh and location of the building is shown in Fig. 6. The beam element is now activated in the analysis to simulate the building. It should be noted that from the plan view shown in Fig. 1, if the building is included in the simulation the numerical mesh is no longer symmetrical. With relatively large excavation width, based on the engineering judgment the building may locally affect the settlement pattern only on its side not the overall excavation responses as well as the building on the other side. Since this study focuses only on the deformation characteristics of building I, only a half-mesh model with the interested building is adopted for simplicity. In addition, field measurements were only available for the rear building shown in Fig. 6. Thus, only that part of the analytical results is studied.

Figure 9(a) demonstrates the influences of building stiffness on the building deformation when the building weight is not considered. It indicated that the existing of the structure does obviously reform the settlement trough beneath the structure in which the lower stiffness building exhibits more flexible deformation. Moreover, the lower stiffness conditions may also result in larger settlement at two ends and smaller settlement in the middle portion of the structure than the original rigidity case. These observations are consistent with those of Potts and Addenbrooke (1997). Furthermore, the predicted settlements appear underestimated for every stiffness condition. Therefore, it leaves a possibility in which the building settlement could be better predicted if the weight is included.

Figure 9(b) indicates the predicted building settlement at various rigidities when the building weight is included. Clearly, the analytical deformation troughs become closer to the real observation. Although deviation still exists between the observation and prediction, the numerical results exhibit that to obtain better analytical building settlement the building weight should be taken into account in the analysis. Moreover, the building stiffness should be reduced from the original method to capture properly the real flexible building deformation.

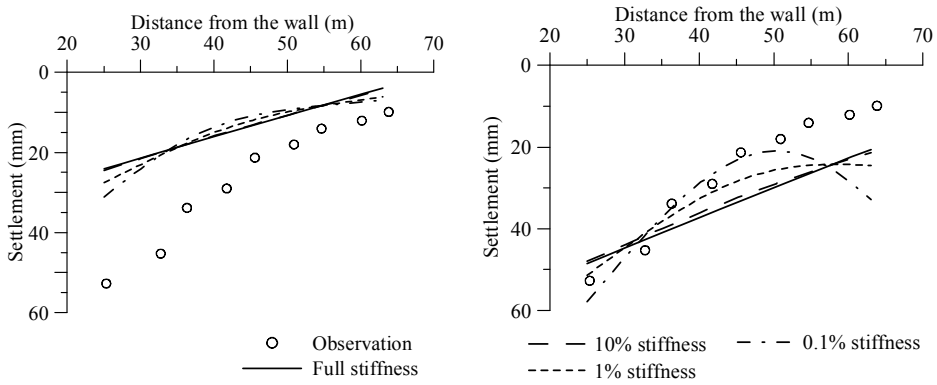

(a) Weightless beam (b) Weight beam

Fig. 9 Building deformation at various building stiffness

5. CONCLUDING REMARKS

This paper discusses the behavior of zoned excavation and the response of a neighboring structure by utilizing field measurements and analytical results of a studied case. Findings from this study offer valuable insights regarding the wall and ground responses and the building simulation technique. Herein, several conclusions can be drawn:

1. The field measurements indicate that the wall and ground movement characteristics of the zoned excavation are similar to those of conventional excavation method. In other words, the zoned excavation behavior in terms of deformation pattern and displacement amplitude can be evaluated using the empirical relationships reported in the literature.
2. The ratio between the building subsidence and the surface ground settlement along its range may vary within a relatively small scale. It varies roughly from 2 to 4 for the low rise concrete framed building in this study.
3. The simplified method proposed by Potts and Addenbrooks (1997) that simulates the building as a weightless beam on the ground surface appears inadequate to predict accurate building settlement. However, the results can be significantly improved if the equivalent beam stiffness and the building weight are properly considered. More rigorous building models are warranted to provide better prediction and more in-depth information such as building's tilting or horizontal strain.

REFERENCES

Boone, S. J. (1996). "Ground-movement-related building damage." *Journal of Geotechnical Engineering*, ASCE, **122**(11), 886–896.

Boscardin, M. D. and Cording, E. J. (1989). "Building response to excavation induced settlement." *Journal of Geotechnical Engineering*, ASCE, **115**(1), 1–21.

Burd, H. J., Houlsby, G. T., Augarde, C. E., and Liu, G. (2000). "Modeling tunneling-induced settlement of masonry buildings." *Proc. of the Institution of Civil Engineers: Geotechnical Engineering*, ASCE, **143**, 17–29.

Burland, J. B., Standing, J. R., and Jardine, F. M., (2001). *Building Response to Tunnelling-Case Studies from Construction of the Jubilee Line Extension*, London, Volumes 1-2, Thomas Telford.

Burland, J. B. and Wroth, C. P. (1974). "Settlement of buildings and associated damage." *Proc., Conference on Settlement of Structures*, Cambridge, 611–654.

Dang, H. P., Lin, H. D., and Hsieh, Y. M. (2010). "Simulation of advanced soil models by using user defined model feature in Plaxis." *Proc., 17th Southeast Asian Geotechnical Conference*, Taipei, Taiwan, **1**, 149–152.

Duncan, J. M. and Chang, C. Y. (1970). "Nonlinear analysis of stress and strain in soils." *Journal of the Soil Mechanics and Foundation Division*, ASCE, **96**(5), 637–659.

Finno, R. J., Bryon, S., and Calvello, M. (2002). "Performance of a stiff support system in soft clay." *Geotechnical Engineering and Geoenvironmental Engineering*, ASCE, **128**(8), 660–671.

Hsieh, P. G. and Ou, C. Y. (1997). "Use of the modified hyperbolic model in excavation analysis under undrained condition." *Geotechnical Engineering*, SEAGS, **28**(2), 123–150.

Hsieh, P. G. and Ou, C. Y. (1998). "Shape of ground surface settlement profiles caused by excavation." *Canadian Geotechnical Journal*, **35**(6), 1004–1017.

Hsieh, P. G. and Ou, C. Y. (2011). "Analysis of nonlinear stress and strain in clay under the undrained condition." *Journal of Mechanics*, The Society of Theoretical and Applied Mechanics, **27**(2), 201213.

Hsieh, P. G., Kung, T. C., Ou, C. Y., and Tang, Y. G. (2003). "Deep excavation analysis with consideration of small strain modulus and its degradation behavior of clay." *Proc., 12th Asian Regional Conference on Soil Mechanics and Geotechnical Engineering, Singapore*, **1**, 785–788.

Kung, G. T. C., Hsiao, E. C. L., and Juang, C. H. (2007). "Evaluation of a simplified small-strain soil model for analysis of excavation-induced movements." *Canadian Geotechnical Journal*, **44**, 726–736.

Laefer, D. F., Ceribasi, S., Long, J. H., and Cording, E. J. (2009). "Predicting RC frame response to excavation-induced settlement." *Journal of Geotechnical and Geoenvironmental Engineering*, ASCE, **135**(11), 1605–1619.

Lin, H. D., Dang, H. P., Kung, J. H. S., Hsiung, B. B. C., and Chen, C. H. (2011). "Performance of a zoned excavation and its effect on neighboring buildings." *Proc., 14th Asian Regional Conference on Soil Mechanics and Geotechnical Engineering*, CD-ROM, 327, Hong Kong.

Lin, H. D., Ou, C. Y., and Wang, C. C. (2002). "Time-dependent displacement of diaphragm wall induced by soil creep." *Journal of the Chinese Institute of Engineers*, **25**(2), 223–231.

Ou, C. Y. (2006). *Deep Excavation-Theory and Practice*, Taylor & Francis, The Netherlands.

Ou, C. Y., Liao, J. T., and Cheng, W. L. (2000). "Building response and ground movements induced by a deep excavation." *Géotechnique*, **50**(3), 209–220.

Ou, C. Y., Liao, J. T., and Lin, H. D. (1998). "Performance of diaphragm wall constructed using top down method." *Journal of Geotechnical Engineering and Geoenvironmental Engineering*, ASCE, **124**(9), 798–808.

Potts, D. M. and Addenbrooke, T. I. (1997). "A structure's influence on tunneling-induced ground movements." *Proc. of the Institution of Civil Engineers: Geotechnical Engineering*, **125**, 109–125.

Schuster, M., Kung, G. T. C., Juang, C. H., and Hashash, Y. M. A. (2009). "Simplified model for evaluating damage potential of building adjacent to a braced excavation." *Journal of Geotechnical and Geoenvironmental Engineering*, ASCE, **135**(12), 1823–1835.

Son, M. and Cording, E. J. (2005). "Estimation of building damage due to excavation-induced ground movements." *Journal of Geotechnical and Geoenvironmental Engineering*, ASCE, **131**(2), 162–177.

Wong, K. S. and Brom, B. B. (1989). "Lateral wall deflections a braced excavation in clay." *Journal of Geotechnical Engineering*, ASCE, **115**(6), 853–870.